SLOTLINES

The propagation and radiation of high frequency signals are getting more important as the technology progresses. For example, the clock rate for digital circuitry is over hundreds of megahertz. The booming wireless applications have pushed the low cost and high volume products to the gigahertz range. Engineers need to understand the behavior of high frequency signals to have a proper and efficient layout when they design a new circuit. This article introduces one type of high frequency transmission lines called the slotline. The configuration, terminology, analysis, and applications are discussed in subsequent sections.

A slotline is an uniplanar wave-guiding structure proposed by Cohn in 1968 (1). Figure 1(a) shows the basic configuration of a slotline. It consists of a narrow slit between two metal planes that are on one side of the substrate. It is different from a microstrip line that has a strip and a ground plane on the opposite sides of a substrate. The substrate property (μ, ϵ) and thickness h, the slot width w, and the metal thickness t are parameters determining slotline characteristics. The electromagnetic fields of a slotline concentrate around the slot region and propagate along the longitudinal direction as depicted in Fig. 1(b). The main electric field lines are on the transverse plane, and there are more lines in the substrate region because it has a higher dielectric constant. The propagation mode is nontransverse electromagnetic (non-TEM). Unlike the non-TEM metal waveguide, the slotline has no cut-off frequency because it has two separated metals. We will use the spectral domain approach to analyze the slotline. The propagation constant and the characteristic impedance are obtained from this rigorous analysis.

Microwave circuits are frequently packaged in a metal shield. That is, the bottom of the substrate in Fig. 1(a) is attached to a metal plane. Figure 2 shows a conductor-backed slotline (CBSL). The additional bottom ground plane provides better mechanical strength and heat-sinking ability. However, the presence of the conductor backing can cause a serious problem, which is power leakage in the transverse direction. This power loss results in undesirable package and crosstalk effects. The leakage phenomenon is easy to understand. Besides the slotline mode, the conductor-backed slot-

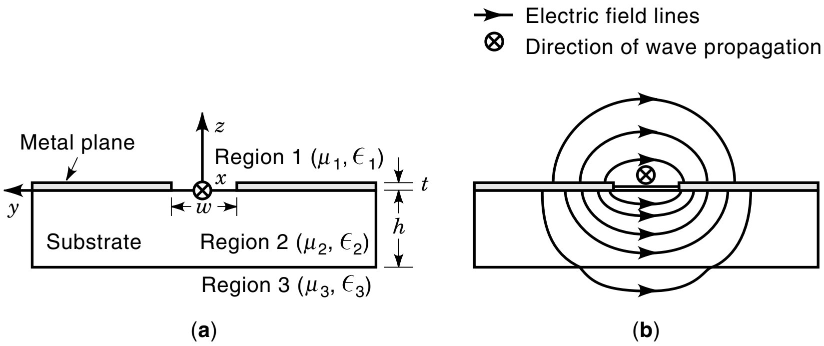

Figure 1. Slotline configuration: (a) cross-sectional view, (b) electric field distribution and wave direction.

line also supports a parallel-plate mode in a region away from the open slit. A slotline mode is a non-TEM wave and has its fields spread in both the substrate and air regions. A parallel-plate mode is a TEM wave and has all its energy confined in the substrate between two metal planes. Therefore, the effective dielectric constant of a parallel-plate mode is always higher than that of a slotline mode. Under these circumstances, the parallel-plate mode behaves as the dominant mode, and the slotline mode is the first higher-order mode on the dispersion curves. Therefore, the energy in the slotline mode tends to leak to the parallel-plate mode. This leaky energy propagates at an angle with the longitudinal direction and is frequency-dependent. A rigorous analysis to predict the leaky performance and some methods to reduce the energy loss are discussed in the subsequent section.

Slotlines can be built using the same fabrication process for the microstrip line and the coplanar waveguide (CPW). All these transmission lines have planar in geometries and are very useful in integrated circuit designs. The easy integration of these structures on a substrate provides an additional design choice. It becomes important to understand completely the transition between different transmission lines. Slotline discontinuities, coaxial-to-slotline, microstrip-to-slotline, and CPW-to-slotline transitions are investigated in this article. Compared with a microstrip line and a CPW, the slotline has high dispersive characteristics and a divergent field distribution. Therefore, the slotline is not commonly used as a long transmission line but rather as a short high-impedance line or a radiating geometry. As another application, the slotline has an elliptically polarized magnetic field that makes it suitable for use with a ferromagnetic material to build a nonreciprocal device (2).

THEORETICAL ANALYSIS

Several methods can be used to analyze a uniform slotline. They range from a closed form expression, a quasi-static approach, to full-wave frequency- and time-domain approaches

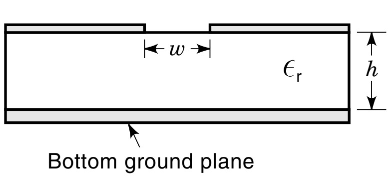

Figure 2. Conductor-backed slotline that has a good mechanical strength and heat-sinking capability.

(3–9). The closed form and quasi-static approach are time efficient but have limited accuracy. The rigorous full-wave methods, on the other hand, provide accurate data with a lengthy formulation and programming process. Due to the progress in computer technology, a well-written simulation code can give complete characteristics of a transmission line within few minutes on a personal computer. We will concentrate on one of the most versatile numerical methods called spectral domain analysis, and also known as the spectral domain approach (SDA) (10). This technique is very efficient in analyzing multilayered planar structures. Moreover, the same formulation can be extended to analyze circuit discontinuities. Readers who are interested in closed form expressions can refer to Ref. 11.

Spectral Domain Analysis

Formulation of the Dyadic Green's Function. Figure 1(a) shows a single-layered slotline with its coordinate system. The metal and substrate extend into infinity in the transverse, $\pm y$, direction. The wave propagates along the $+x$ direction. The conductor thickness t and loss from metal and dielectric are neglected in the following derivation. We can easily extend the procedures to a multilayered and lossy slotline. The formulation is based on the concept of Hertz potentials (10,12). If we define TE-to-z and TM-to-z Hertz potentials as ϕ_i^e and ϕ_i^h, the field components can be expressed as

$$E_{xi}(x,y,z) = \frac{\partial^2 \phi_i^e(x,y,z)}{\partial x \partial z} - j\omega\mu_i \frac{\partial \phi_i^h(x,y,z)}{\partial y} \tag{1a}$$

$$E_{yi}(x,y,z) = \frac{\partial^2 \phi_i^e(x,y,z)}{\partial y \partial z} + j\omega\mu_i \frac{\partial \phi_i^h(x,y,z)}{\partial x} \tag{1b}$$

$$E_{zi}(x,y,z) = \left(\frac{\partial^2}{\partial Z^2} + k_i^2\right)\phi_i^e(x,y,z) \tag{1c}$$

$$H_{xi}(x,y,z) = j\omega\epsilon_i \frac{\partial \phi_i^e(x,y,z)}{\partial y} + \frac{\partial^2 \phi_i^h(x,y,z)}{\partial x \partial z} \tag{1d}$$

$$H_{yi}(x,y,z) = -j\omega\epsilon_i \frac{\partial \phi_i^e(x,y,z)}{\partial x} + \frac{\partial^2 \phi_i^h(x,y,z)}{\partial y \partial z} \tag{1e}$$

$$H_{zi}(x,y,z) = \left(\frac{\partial^2}{\partial Z^2} + k_i^2\right)\phi_i^h(x,y,z) \tag{1f}$$

$$k_i = \omega\sqrt{\mu_i \epsilon_i} \tag{1g}$$

where a harmonic time dependence of $e^{j\omega t}$, $\omega = 2\pi f$, is assumed and i = 1, 2, and 3 refer to regions 1, 2, and 3, respectively.

ϵ_i and μ_i are the electric permittivity and magnetic permeability of each region. Hertz potentials satisfy the Helmholtz wave equation

$$(\nabla^2 + k_i^2)\phi_i^{e,h} = 0 \tag{2}$$

Equations (1a)–(1f) and (2) are second-order partial differential equations. However, they can be simplified into ordinary differential equations by (1) assuming the x-dependence as $e^{-j\alpha x}$ and (2) defining the spatial Fourier transform in the y direction as

$$\tilde{\phi}_i^{e,h}(\beta, z) = \sum_{-\infty}^{\infty} \phi_i^{e,h}(y, z)e^{j\beta y}\, dy \tag{3}$$

With these definitions, the transformed fields of Eqs. (1a)–(1f) and (2) are

$$\tilde{E}_{xi}(\beta, z) = -j\alpha\frac{d\tilde{\phi}_i^e}{dz} - \omega\mu_i\beta\tilde{\phi}_i^h \tag{4a}$$

$$\tilde{E}_{yi}(\beta, z) = -j\beta\frac{d\tilde{\phi}_i^e}{dz} + \omega\mu_i\alpha\tilde{\phi}_i^h \tag{4b}$$

$$\tilde{E}_{zi}(\beta, z) = \left(\frac{d^2}{dz^2} + k_i^2\right)\tilde{\phi}_i^e \tag{4c}$$

$$\tilde{H}_{xi}(\beta, z) = \omega\epsilon_i\beta\tilde{\phi}_i^e - j\alpha\frac{d\tilde{\phi}_i^h}{dz} \tag{4d}$$

$$\tilde{H}_{yi}(\beta, z) = -\omega\epsilon_i\alpha\tilde{\phi}_i^e - j\beta\frac{d\tilde{\phi}_i^h}{dz} \tag{4e}$$

$$\tilde{H}_{zi}(\beta, z) = \left(\frac{d^2}{dz^2} + k_i^2\right)\tilde{\phi}_i^h \tag{4f}$$

$$\left(\frac{d^2}{dz^2} - \gamma_i^2\right)\tilde{\phi}_i^{e,h}(\beta, z) = 0 \tag{4g}$$

where $\gamma_i^2 = \alpha^2 + \beta^2 - k_i^2$. Equation (4g) is an ordinary second-order wave equation. The general solutions of this wave equation at each region in Fig. 1(a) are

$$\tilde{\phi}_1^e = A_1 e^{-\gamma_1 z} \tag{5a}$$

$$\tilde{\phi}_1^h = A_2 e^{-\gamma_1 z} \tag{5b}$$

$$\tilde{\phi}_2^e = B_1 \sinh[\gamma_2(h+z)] + B_2 \cosh[\gamma_2(h+z)] \tag{5c}$$

$$\tilde{\phi}_2^h = B_3 \sinh[\gamma_2(h+z)] + B_4 \cosh[\gamma_2(h+z)] \tag{5d}$$

$$\tilde{\phi}_3^e = C_1 e^{-\gamma_3(h+z)} \tag{5e}$$

$$\tilde{\phi}_3^h = C_2 e^{-\gamma_3(h+z)} \tag{5f}$$

where A_1, A_2, B_1, B_2, B_3, B_4, C_1, and C_2 are unknown coefficients. All solutions are functions of the spatial variable z only. We use the hyperbolic functions to represent the standing wave nature of fields at the stratified region 2. The decaying feature of energy in air regions above and below the substrate is in the form of an exponential function. Substituting Eqs. (5a)–(5f) in Eqs. (4a)–(4f), we have the general field solutions. There are a total eight unknowns in Eqs. (5a)–(5f). We need eight independent equations to get the dyadic Green's function. The next step is to match the transformed boundary conditions: At $z = -h$,

$$\tilde{E}_{x2} = \tilde{E}_{x3} \tag{6a}$$

$$\tilde{E}_{y2} = \tilde{E}_{y3} \tag{6b}$$

$$\tilde{H}_{x2} = \tilde{H}_{x3} \tag{6c}$$

$$\tilde{H}_{y2} = \tilde{H}_{y3} \tag{6d}$$

At $z = 0$,

$$\tilde{E}_{x1} = \tilde{E}_{x2} = \tilde{e}_x \tag{7a}$$

$$\tilde{E}_{y1} = \tilde{E}_{y2} = \tilde{e}_y \tag{7b}$$

$$\tilde{J}_x = \tilde{H}_{y2} - \tilde{H}_{y1} \tag{7c}$$

$$\tilde{J}_y = \tilde{H}_{y1} - \tilde{H}_{y2} \tag{7d}$$

By eliminating eight unknown coefficients using boundary conditions in Eqs. (6a)–(6d) and (7a)–(7d), we have a set of dyadic Green's function

$$\begin{bmatrix} \tilde{J}_x \\ \tilde{J}_y \end{bmatrix} = \begin{bmatrix} \tilde{G}_{xx} & \tilde{G}_{xy} \\ \tilde{G}_{yx} & \tilde{G}_{yy} \end{bmatrix} \begin{bmatrix} \tilde{e}_x \\ \tilde{e}_y \end{bmatrix} \tag{8}$$

where ($\tilde{e}_x$, $\tilde{e}_y$) and ($\tilde{J}_x$, $\tilde{J}_y$) are electric fields and currents at the slot and the conductor of the $z = 0$ plane, respectively. In the formulation, all unknown coefficients in Eqs. (5a)–(5f) are only functions of two variables ($\tilde{e}_x$, $\tilde{e}_y$). The field characteristic of a slotline is solved if we can find proper functions to describe the slot fields accurately. This task is done using the method of moment (MoM). One such technique, called the Galerkin's method, is discussed in the following section.

Galerkin's Method. To solve the propagation constant α and field distributions, we can use Galerkin's method. The Galerkin method uses the same weighting function as the basis function. Suppose that the aperture electric field is expressed as

$$\tilde{e}_x(\beta) = \sum_{m=1}^{M} a_m \tilde{f}_{xm}(\beta) \tag{9a}$$

$$\tilde{e}_y(\beta) = \sum_{n=1}^{M} b_n \tilde{f}_{yn}(\beta) \tag{9b}$$

where $\tilde{f}_{xm}$ and $\tilde{f}_{yn}$ are complete basis functions with unknown coefficients a_m and b_n. Because the electric fields and currents are nonzero in complementary regions at the interface $z = 0$, we can multiply both sides of Eq. (8) by the complex conjugate of aperture electric fields. Then, integrating the product at $z = 0$, we obtain a set of eigenvalue equations:

$$\begin{bmatrix} \tilde{Z}_{xx} & \tilde{Z}_{xy} \\ \tilde{Z}_{yx} & \tilde{Z}_{yy} \end{bmatrix} = 0 \tag{10}$$

By setting the determinant of Eq. (10) equal to zero, all modes supported by the slotline are solved from the root-searching results of α. The unknown coefficients in Eqs. (9a) and (9b) are also obtained during this process. Substituting the solved

Eqs. (9a) and (9b) into Eqs. (4a)–(4g) and (5a)–(5f), the electric and magnetic fields can be calculated.

Characteristic Impedance. There is no unique definition of characteristic impedance for a non-TEM transmission line. Power-and-current, power-and-voltage, and voltage-and-current are three commonly used definitions in calculating the characteristic impedance. The characteristic impedance of a slotline is usually defined in terms of the power and voltage relation

$$Z_0 = \frac{V^2}{2P_{\text{avg}}} \tag{11}$$

where V is the voltage across the slot. This potential difference is calculated by integrating the electric field

$$V = \int_{\text{slot}} E_y(y)\,dy \tag{12}$$

The time-averaged power P_{avg} propagated along the slotline is

$$P_{\text{avg}} = \frac{1}{4\pi}\text{Re}\int\int[\tilde{E}_y(\beta,z)\tilde{H}_z^*(\beta,z) - \tilde{E}_z(\beta,z)\tilde{H}_y^*(\beta,z)]\,dz\,d\beta \tag{13}$$

where * means the complex conjugate.

Dispersion Behaviors of a Slotline. A computer code based on Eqs. (10) and (11) is written for analyzing a slotline. Figure 3 shows the propagation constant and impedance of a slotline as a function of substrate thickness. As the substrate thickness increases, the effective dielectric constant of a slotline increases because there is more energy in the substrate. Also, the slotline is a slow wave structure because the normalized propagation constant is always greater than one. Besides the characteristics of the dominant mode, a full-wave analysis also provides the information of higher-order, evanescent, and leaky modes (8,11).

Because the fields of a slotline are concentrated around the narrow slot, any parameter changes at this area affect the slotline characteristic. Kitazawa analyzed the effect of finite metal thickness on the slotline performance with the modified SDA (13). He added a narrow, thin air region of the height of the metal thickness into the formulation as shown in Fig. 4. Then two sets of basis functions were set at the top and bottom edges of the narrow slot region. Figure 5 depicts the normalized propagation constant and impedance of a slotline with different metal thicknesses. Because the slot is modeled as an air-filled region, there is increasing energy in the air when the metal thickness increases. Therefore, the propagation constant decreases with increasing metal thickness. Obviously the metal thickness influences the slotline. It is important to incorporate the metal thickness into consideration in designing slot-type transmission lines (e.g., the slotline and the coplanar waveguide).

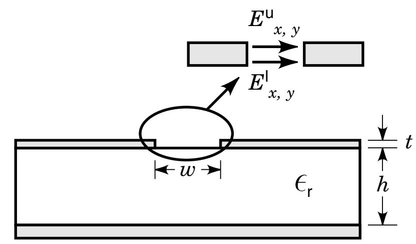

Figure 4. Basis functions used to simulate a slotline with a finite conductor thickness t in SDA.

Choice of Basis Functions (10,12). The accuracy and efficiency of the final solution depend on the accuracy with which the basis functions represent the true electric field. The entire domain basis functions (e.g., the sinusoidal functions or Chebyshev polynomials) are preferred in the analysis of a uniform transmission line. Only two or three terms can yield a very accurate result. On the other hand, the subdomain basis functions (e.g., rectangular and triangular functions) are commonly used in the analysis of circuit discontinuities. Table 1 compares the results of using the entire and subdomain basis functions in analyzing a uniform slotline.

Leaky Phenomenon and Control on Conductor-Backed Slotline

Recently some work has been done to investigate and reduce the leaky phenomena in various planar structures (14–19).

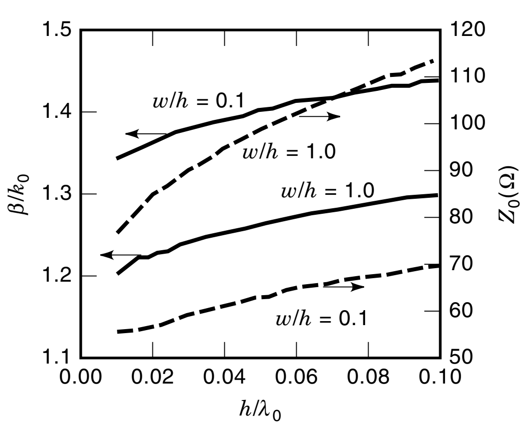

Figure 3. Normalized propagation constant and characteristic impedance of slotline (ϵ_r = 4.5). The slotline characteristics are determined by its constituent parameters.

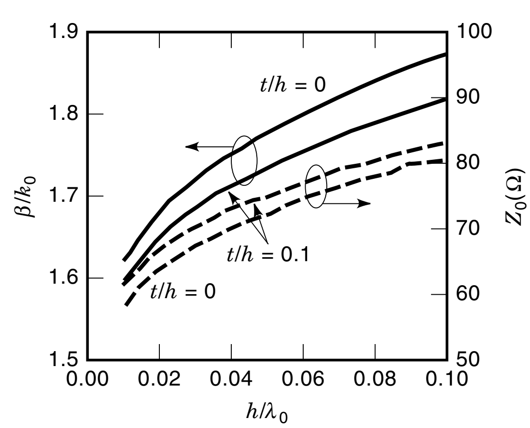

Figure 5. Normalized propagation constant and characteristic impedance of slotline with different conductor thickness (ϵ_r = 10.5, w/h = 0.5). The conductor thickness has an obvious influence on slotline performance.

Table 1. Analysis of a Uniform Slotline[a]

Number of Basis Function	Entire Domain Function	Subdomain Function
1	1.9083	1.8977
2	1.8715	1.8795
3	1.8695	1.8751
4	1.8693	1.8734
5	1.8692	1.8725
10	1.8692	1.8708

[a] The entire domain function is more suitable in analyzing a uniform slotline.

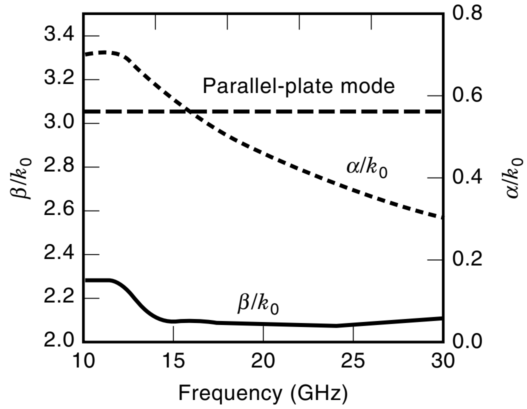

Figure 7. Normalized propagation constant of CBSL and parallel-plate mode. $\epsilon_r = 9.5$, $h = 1$ mm, $w = 0.25$ mm. There is a nonzero attenuation constant because the phase constant of a slotline is always less than that of a parallel-plate mode.

This power leakage in terms of other guided waves is an interesting behavior and can be analyzed easily with a little modification on the conventional SDA. The integration path of a conventional SDA is along the real axis of the spectral variable β. In order to include the contribution of leaky waves, special attention should be paid to the integration path (20). For a leaky transmission line, the model field is no longer bounded, and the propagation constant becomes complex instead of real. Therefore, a deformed integration path or residual calculation is commonly used to handle the leaky waves as depicted in Fig. 6. The deformed integration path is numerically easily implemented. However, it suffers from the numerical divergence when the integration path is close to leaky-wave poles. In this case, the residue calculation is preferred for an accurate and general formulation.

Leaky Phenomenon. The conductor-backed slotline shown in Fig. 2 has the inherent problem of power leakage in the transverse direction. This is so because the slotline mode of a CBSL has a lower effective dielectric constant than that of a parallel-plate mode. Figure 7 depicts the dispersion curves for both modes. Clearly, the phase constant of the slotline mode is always less than that of a parallel-plate mode. With the complex root-searching method, the attenuation constant (the imaginary part of α) exists over all frequencies. It says that the guided slotline mode loses energy when it propagates. The leakage phenomenon is also frequency-dependent. Shigesawa et al. conducted a comprehensive analysis and measurement of this issue (14).

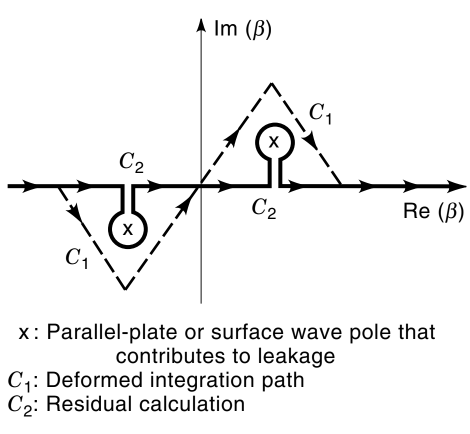

Figure 6. Integration paths in the spectral domain analysis to calculate the leaky wave-guiding structures.

Leakage Control. The leakage problem shadows the CBSL. It is important to eliminate or reduce the power leakage that causes unwanted coupling and energy loss. Figure 8 depicts some proposed configurations to control the power leakage (15–17). The basic idea is to make the effective dielectric constant of the slotline mode higher than that of a parallel-plate mode with the additional dielectric compensation [Fig. 8(a,b)]. Or, we can physically confine the fields within the slot region using metal vias in the substrate [Fig. 8(c)]. Figure 8(a) can be easily analyzed using the SDA. Figure 9 demonstrates the leakage control of a CBSL with a proper material combination. It must be pointed out that the leaky phenomenon is caused by the so-called LSM mode in Fig. 8(a) because there are two substrates between metal plates. The attenuation becomes zero when the propagation constant of a slotline is higher than the LSM mode. There is a transition region between then leaky and nonleaky regions. Some researchers have studied this microscopic picture of mode transitions (21,22).

Slotline Discontinuities

The short end and the open end are two single-ended slotline discontinuities. These two discontinuities are frequently used as parts of slotline components. Their characteristics are, therefore, important for understanding the component behavior.

Short End. The short end is realized by connecting one end of the slotline shown in Fig. 1 with metallization. This discontinuity has been analyzed both theoretically and experimentally (23–25). Figure 10 plots the comparison for the normalized end reactance. The short-end slotline exhibits inductive loading because the reactance is positive. It means that the stored energy is mainly in the form of magnetic energy. Besides the reactive energy, there is a radiation and surface wave loss caused by this discontinuity. The loss makes the reflection coefficient less than one, which can be modeled as a resistor in the equivalent circuit. Figure 11 shows the normalized resistance of a shorted slotline using a full-wave analysis technique (25). Figures 10 and 11 say that the induc-

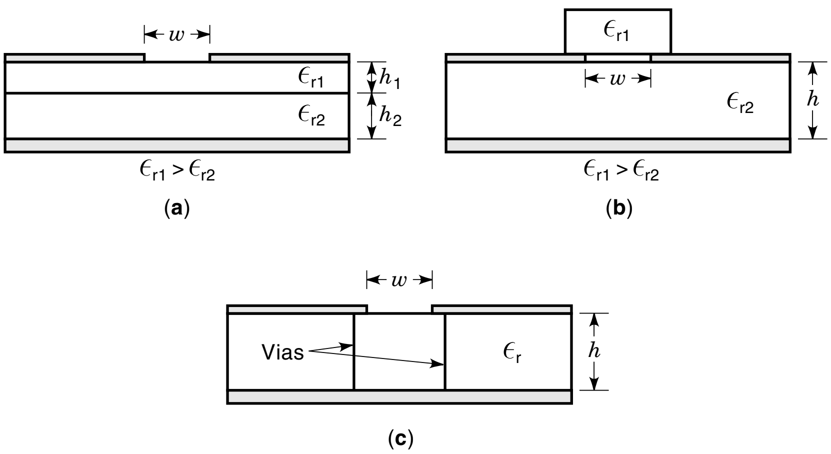

Figure 8. Configurations to reduce or eliminate the leakage on a CBSL: (a) with an additional substrate layer, (b) with a superstrate for dielectric compensation, (c) with periodic vias in the substrate.

tive loading and the radiation loss gets stronger as the frequency increases.

Open End. Unlike the microstrip line, an open-ended slotline is difficult to realize and is sometimes impractical in circuit applications. Figure 12 depicts some variations of an open-ended slotline. There is a very strong radiation loss for the configurations in Fig. 12(a,b). Although it is not a good candidate in circuit applications, Fig. 12(b) is commonly used in the end-fired antenna design. Figures 12(c,d) have confined energy and are experimentally studied by Chramiec (26). If the operating frequency is higher than the resonant frequency of the disk resonator, Fig. 12(c,d) behaves like an open circuit.

Transitions

Transitions between the slotline and other wave-guiding structures extend the design and test capabilities of a slotline. For example, a coaxial-to-slotline transition is needed to test the slotline in a standard microwave measurement system. There are several different ways to combine two transmission lines. The one with a natural field match at the junction region gives maximum energy transfer. That is, for a good transition, the orientations of electric and magnetic fields should match each other. In the following sections, we will discuss several practical transitions.

Coaxial-to-Slotline Transition. Most microwave measurement systems use the coaxial cable as the input/output (I/O) transmission line. It needs a good coaxial-to-slotline transition to test the slotline performance. Figure 13 depicts the coaxial-to-slotline transition. These two structures cross each other with a right angle to have the proper field match. The center conductor of the coaxial line is connected to one of the slotline metal planes, and the outer conductor is connected to the other one. With the open end at one side of the slotline, the energy propagates along the uniform section. This configuration is also useful in exciting a slotline antenna, which is a double short-ended slotline. Knorr analyzed and measured this transition with a 50 Ω microstrip line and a 75 Ω slotline (27). It has a good voltage standing-wave ratio (VSWR) for frequencies less than 4 GHz. The performance of the transition gets worse at higher frequencies.

The open end of the slotline shown in Fig. 13 may cause unwanted radiation loss. Although it has low return loss, it does not mean that there is a maximum energy transfer in the form of a guided wave. To reduce this radiation loss, a movable short-end configuration is proposed (11). Because of

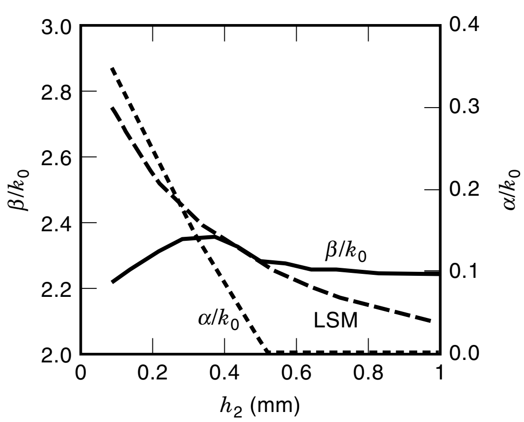

Figure 9. Normalized propagation constant of a nonleaky CBSL with an additional substrate layer. $\epsilon_{r1} = 9.5$, $\epsilon_{r2} = 2.33$, $h_1 = 1$ mm, $w = 0.25$ mm, frequency = 20 GHz. The attenuation constant becomes zero when the phase constant of a slotline is higher than that of a LSM.

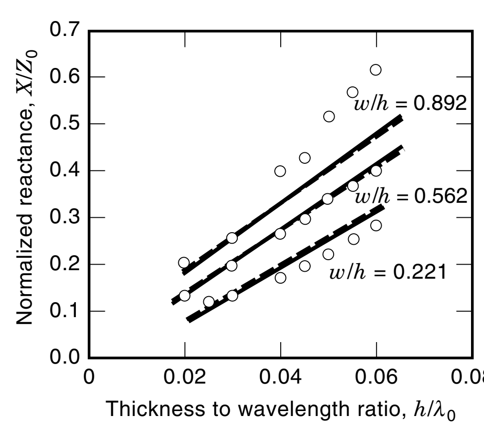

Figure 10. Normalized end reactance of a shorted slotline, $\epsilon_r = 12$. The shorted slotline is inductively loaded. Dots are measured data; solid and dashed lines are calculated results. (Reprinted with permission from Ref. 25, © 1988 IEEE.)

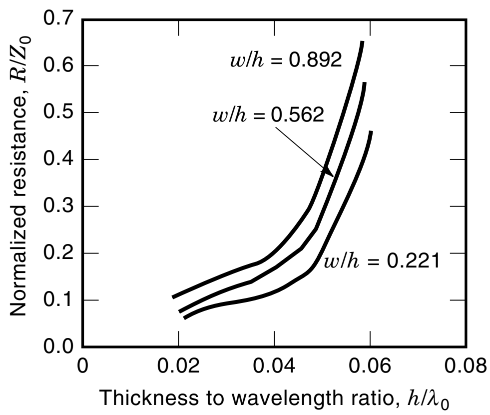

Figure 11. Normalized end resistance of a shorted slotline, ϵ_r = 12. This resistance represents the energy loss of a shorted slotline. (Reprinted with permission from Ref. 25, © 1988 IEEE.)

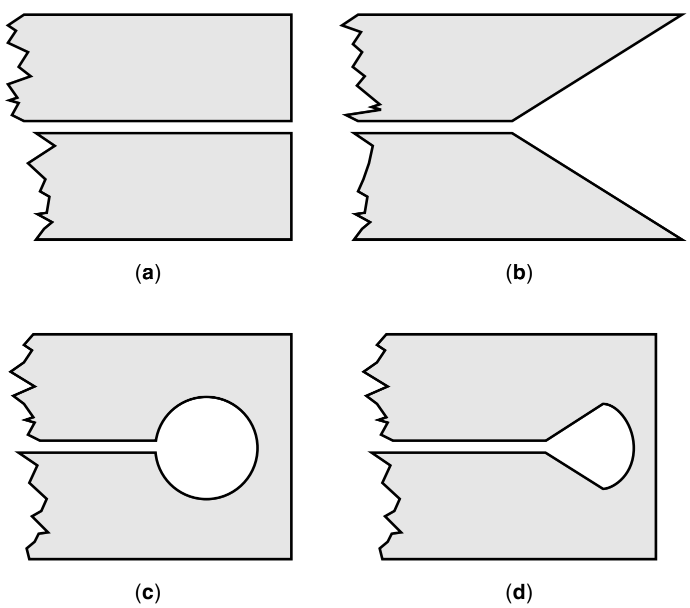

Figure 12. Various structures for slotline open end: (a) an abrupt discontinuity; (b) with a flared angle; (c) with a circular disk; and (d) with a flared slot and half-disk (Reprinted with permission from *Microstrip Lines and Slotlines* by K. C. Gupta et al., Artech House, Inc., Norwood, MA, USA. http://www.artech-house.com.)

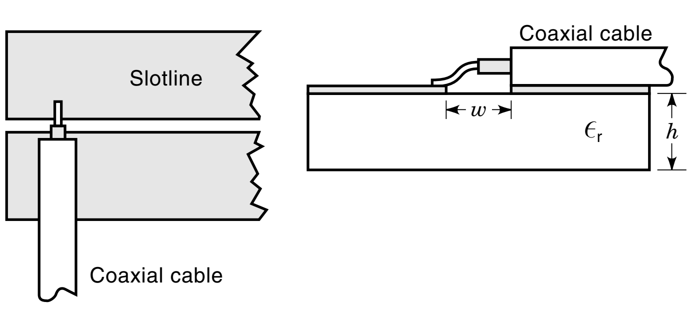

Figure 13. Coaxial-to-slotline transition. (Reprinted with permission from Ref. 27, © 1974 IEEE.)

the resonant wavelength, this type of transition has an optimal VSWR over a narrow frequency range.

Microstrip-to-Slotline Transition. Microstrip circuits are most widely used in microwave integrated circuits. The microstrip-to-slotline transition expands applications for both the microstrip line and the slotline. Also the fabrication is very easy and accurate by etching the metallization on both sides of the substrate. It makes the double-sided circuit design feasible. A branch-line coupler based on this transition has been demonstrated (28). Figure 14 shows the transition with both lines crossing at a right angle and extending about a quarter wavelength beyond each other. Chambers et al. used an approximate transmission line method to analyze this transition (29). More rigorous full-wave methods were also reported (25,30,31). All simulations agree well with the experiment done by Knorr at the lower frequency, but there is a large discrepancy at the high-frequency end. The deviation may be caused by fabrication tolerance. Besides, the substrate used in the experiment (27) is Custom Hik 707-20 (ϵ_r = 20), which is usually very lossy at higher frequencies. This loss parameter was not included in the previously mentioned simulations.

Figure 14 is a narrow-band transition. The bandwidth limitation is a result of the frequency dependence of the quarter wavelength sections. Several papers have tried to improve the bandwidth with different approaches (32–35). It is found that the bandwidth is related to the stub reactance and impedance. The lowest VSWR occurs when the reactances cancel each other for the quarter wavelength sections. Moreover, there is a maximum bandwidth when the characteristic impedance of the microstrip stub is 2.618 times the characteristic impedance of the slotline stub (35).

Coplanar Waveguide-to-Slotline Transition. Unlike the microstrip-to-slotline transition, the coplanar waveguide (CPW)-to-slotline transition can be built on the same side of metallization. This configuration is preferred in the monolithic microwave integrated circuits (MMICs), where all metals are on one side of the substrate only. Much effort has been made to study this transition (36–39). Figure 15 shows some of the representative configurations. Figure 15(a) is a CPW-to-slotline T-junction that behaves like a power divider. Two output ports on the slotline are available in Fig. 15(a). If a single output is necessary, the other port can be shorted at a quarter wavelength from the junction. The bonding wire is used to suppress the unwanted mode on the CPW. To increase the bandwidth, a radial stub is used as shown in Fig. 15(b), even though it requires a large circuit space. It is found that Fig.

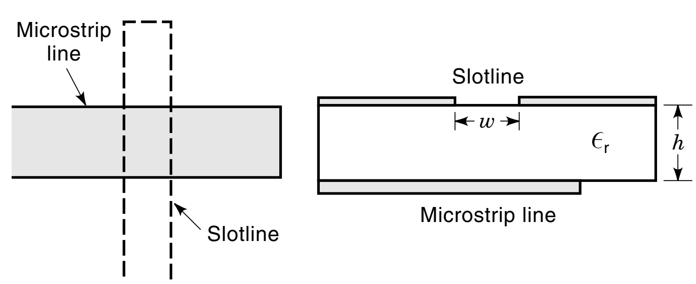

Figure 14. Microstrip-to-slotline transition.

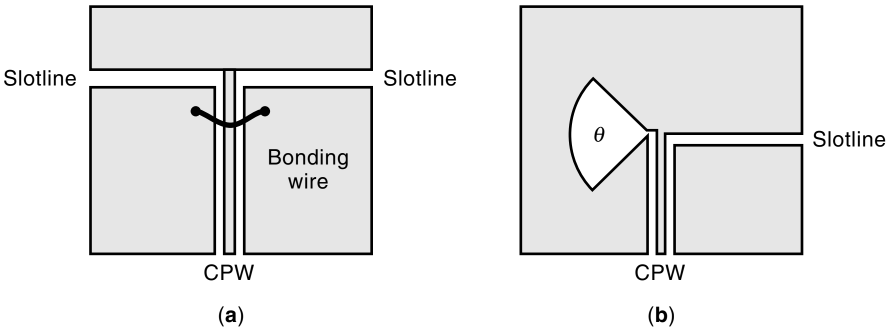

Figure 15. CPW-to-slotline transitions: (a) two slotline outputs, (b) single slotline output. (Reprinted with permission from Refs. 36 and 39, © 1987 and 1993 IEEE.)

15(b) has the best performance in terms of bandwidth and return loss (39). The 1 dB insertion loss bandwidth for this transition is more than 5.2 : 1. Unlike coaxial- and microstrip-to-slotline transitions discussed previously, one design advantage of this transition is that the I/O lines can have an angle from 0° to 90°. The optimal transition can be obtained with a modification of circuit dimensions.

BIBLIOGRAPHY

1. S. B. Cohn, Slotline on a dielectric substrate, *IEEE Trans. Microw. Theory Tech.,* **MTT-17**: 768–778, 1969.
2. L. Courtois and M. de Vecchis, A new class of non-reciprocal components using slotline, *IEEE Trans. Microw. Theory Tech.,* **MTT-23**: 511–516, 1975.
3. R. Garg and K. C. Gupta, Expressions for wavelength and impedance of slotline, *IEEE Trans. Microw. Theory Tech.,* **MTT-24**: 532, 1976.
4. R. Janaswamy and D. H. Schaubert, Characteristic impedance of a wide slotline on low permittivity substrate, *IEEE Trans. Microw. Theory Tech.,* **MTT-34**: 900–902, 1986.
5. J. B. Knorr and K. D. Kuchler, Analysis of coupled slots and coplanar strips on dielectric substrates, *IEEE Trans. Microw. Theory Tech.,* **MTT-23**: 541–548, 1975.
6. T. Itoh and R. Mittra, Dispersion characteristics of slotlines, *Electron. Lett.,* **7**: 364–365, 1971.
7. R. Janaswamy and D. H. Schaubert, Dispersion characteristics for wide slotlines on low permittivity substrate, *IEEE Trans. Microw. Theory Tech.,* **MTT-33**: 723–726, 1985.
8. J. Citerne, S. Toutain, and L. Raczy, Fundamental and higher order modes in microslot lines, *Proc. 5th Eur. Microw. Conf.,* pp. 273–277, 1975.
9. G. C. Liang, Y.-W. Liu, and K. K. Mei, Full-wave analysis of coplanar waveguide and slotline using the time-domain finite-difference method, *IEEE Trans. Microw. Theory Tech.,* **MTT-37**: 1949–1957, 1989.
10. T. Itoh, *Numerical Techniques for Microwave and Millimeter-Wave Passive Structures,* New York: Wiley, 1989.
11. K. C. Gupta et al., *Microstrip Lines and Slotlines,* 2nd ed., Norwood, MA: Artech House, 1996.
12. B. Bhat and S. K. Koul, *Analysis, Design and Applications of Fin Lines,* Norwood, MA: Artech House, 1987.
13. T. Kitazawa, Y. Hayashi, and M. Suzuki, Analysis of the dispersion characteristics of slot line with thick metal coating, *IEEE Trans. Microw. Theory Tech.,* **MTT-28**: 387–392, 1980.
14. H. Shigesawa, M. Tsuji, and A. A. Oliner, Conductor-backed slotline and coplanar waveguide: Dangers and full-wave analysis, *IEEE MTT-S Int. Microw. Symp. Dig.,* **1**: 199–202, 1988.
15. Y. Liu and T. Itoh, Control of leakage in multilayered conductor-backed coplanar structures, *IEEE MTT-S Int. Microw. Symp. Dig.,* **1**: 141–144, 1994.
16. J.-W. Huang and C.-K. C. Tzuang, Mode-coupling-avoidance of shielded conductor-backed coplanar waveguide (CBCPW) using dielectric lines compensation, *IEEE MTT-S Int. Microw. Symp. Dig.,* **1**: 149–152, 1994.
17. N. K. Das, Two conductor-backed configurations of slotline or coplanar waveguide for elimination or suppression of the power-leakage problem, *IEEE MTT-S Int. Microw. Symp. Dig.,* **1**: 153–156, 1994.
18. D. Nghiem et al., Leakage of the dominant mode on stripline with a small air gap, *IEEE Trans. Microw. Theory Tech.,* **MTT-43**: 2549–2556, 1995.
19. N. K. Das, Spectral-domain analysis of complex characteristic impedance of a leaky conductor-backed slotline, *IEEE MTT-S Int. Microw. Symp. Dig.,* **1**: 1791–1794, 1996.
20. C.-Y. Lee et al., Analysis and application of non-leaky uniplanar structures with conductor backing, *J. Microw. Millimeter-Wave Comput. Aided Eng.,* **6**: 319–327, 1996.
21. Y.-D. Lin, J.-W. Sheen, and C.-Y. Chang, Surface-wave leakage properties of coplanar strips, *IEEE MTT-S Int. Microw. Symp. Dig.,* **1**: 229–232, 1995.
22. H. Shigesawa, M. Tsuji, and A. A. Oliner, Simultaneous propagation of bound and leaky dominant modes on printed-circuit lines: A new general effect, *IEEE Trans. Microw. Theory Tech.,* **MTT-43**:3007–3019, 1995.
23. J. B. Knorr and J. Saenz, End effect in a shorted slot, *IEEE Trans. Microw. Theory Tech.,* **MTT-21**: 579–580, 1973.
24. R. Jansen, Hybrid mode analysis of end effects of planar microwave and millimeter wave transmission lines, *Proc. Inst. Elec. Eng.,* **128**: 77–86, 1981.
25. H. Yang and N. G. Alexopoulos, A dynamic model for microstrip-slotline transition and related structures, *IEEE Trans. Microw. Theory Tech.,* **MTT-36**: 286–293, 1988.
26. J. Chramiec, Reactances of slotline short and open circuits on alumina substrate, *IEEE Trans. Microw. Theory Tech.,* **MTT-37**: 1638–1641, 1989.
27. J. B. Knorr, Slotline transitions, *IEEE Trans. Microw. Theory Tech.,* **MTT-22**: 548–554, 1974.
28. C.-Y. Lee and T. Itoh, Full-wave analysis and design of a new double-sided branch-lines coupler and its complementary structure, *IEEE Trans. Microw. Theory Tech.,* **MTT-43**: 1895–1901, 1995.
29. D. Chambers et al., Microwave active network synthesis, *Semiannual Report, Stanford Res. Inst.,* June 1970.
30. Y. M. M. Antar, A. K. Bhattcharyya, and A. Ittipiboon, Microstrip-slotline transition analysis using the spectra domain technique, *IEEE Trans. Microw. Theory Tech.,* **MTT-40**: 515–523, 1992.

31. N. K. Das, Generalized multiport reciprocity analysis of surface-to-surface transitions between multiple printed transmission lines, *IEEE Trans. Microw. Theory Tech.,* **MTT-41**: 1164–1177, 1993.
32. G. H. Robinson and J. L. Allen, Slotline application to miniature ferrite devices, *IEEE Trans. Microw. Theory Tech.,* **MTT-17**: 1097–1101, 1969.
33. F. C. de Ronde, A new class of microstrip directional couplers, *IEEE MTT-S Int. Microw. Symp. Dig.,* **1**: 184–189, 1970.
34. A. Podcameni and M. L. Coimbra, Slotline-microstrip transition on iso/anisotropic substrate: A more accurate design, *Electron. Lett.,* **16**: 780–781, 1980.
35. B. Schuppert, Microstrip/slotline transitions: Modeling and experimental investigations, *IEEE Trans. Microw. Theory Tech.,* **MTT-36**: 1272–1282, 1988.
36. H. Ogawa and A. Minagawa, Uniplanar MIC balanced multiplier—A proposed new structure for MICs, *IEEE Trans. Microw. Theory Tech.,* **MTT-35**: 1363–1368, 1987.
37. W. Grammer and K. S. Yngvesson, Coplanar waveguide transitions to slotline: Design and microprobe characterization, *IEEE Trans. Microw. Theory Tech.,* **MTT-41**: 1653–1658, 1993.
38. T. Q. Ho and S. M. Hart, A broad-band coplanar waveguide to slotline transition, *IEEE Microw. Guided Wave Lett.,* **2**: 415–416, 1992.
39. C. H. Ho, L. Fan, and K. Chang, Broad-band uniplanar hybrid-ring and brach-line couplers, *IEEE Trans. Microw. Theory Tech.,* **MTT-41**: 2116–2125, 1993.

CHUNG-YI LEE
Qualcomm, Inc.
TATSUO ITOH
UCLA Department of Electrical Engineering